Predicting Gabal Gattar Uranium Content as a Function of Total Gamma-ray and Thorium Contents using an Artificial Neural Network in Northeastern Desert, Egypt

Abdelrahem Embaby[1, *], Sayed Gomaa[1], Yehia Darwish[1,2], and Samir Selim[1]

1. Mining and Petroleum Engineering Department, Faculty of Engineering, Al-Azhar University, Cairo, Egypt.
2. Nuclear Materials Authority, P.O. 530 El-Maadi, Cairo, Egypt

Article Info	Abstract
	This study aims to develop an empirical correlation model for estimating the uranium content of the G-V in the Gabal Gattar area, northeastern desert of Egypt, as a function of the thorium content and the total gamma rays. Using the recent MATLAB software, the effect of selecting tan-sigmoid as a transfer function at various numbers of hidden neurons was investigated to arrive at the optimum Artificial Neural Network (ANN) model. The pure-linear function was investigated as the output function, and the Levenberg-Marquardt approach was chosen as the optimization technique. Based on 1221 datasets, a novel ANN-based empirical correlation was developed to calculate the amounts of uranium (U). The results show a wide range of uranium content, with a determination coefficient ($R2$) of about 0.999, a Root Mean Square Error (RMSE) equal to 0.115%, a Mean Relative Error (MRE) of -0.05%, and a Mean Absolute Relative Error (MARE) of 0.76%. Comparing the obtained results with the field investigation shows that the suggested ANN model performed well.

1. Introduction

Artificial neural networks (ANNs) are presently utilized in a wide range of applications like reserve estimation, optimal estimation, real-time data analysis, non-linear problems, and problem prediction. ANNs are data processing systems that consist of a large number of interconnected processing elements that simulate biological neural networks. 5 models of ANNs are being used for a wide variety of tasks in many different fields of business, industry, and science, particularly mining and geology. In this technique, there is one input and one output layer, and at least one hidden layer that permits ANNs to define non-linear systems [1] and [2].

Natural radiations are generally divided into two categories: terrestrial and cosmic. The most significant naturally occurring radioisotopes are those from U^{238} and Th^{232}, as well as their breakdown products. These radionuclides are found at variable concentrations in the Earth's crust. As a result, natural radiation varies from one location to another, with minimal variances [3], [4] and [5].

In the field of mining and geology, many researchers have used ANNs as a new technique for determining and forecasting the ore grade [5-16].

Based on the remote sensing and mineral exploration data put in a GIS database [6] suggested a back-propagation ANN model to determine the high-grade gold zones and potential in the Rodalquilar gold field, south-east Spain. A neural network model with three hidden units the trained network efficiently predicted a gold potential map, showing a good agreement with the available data. [7] used ANNs to evaluate the distribution of Fe content within the iron ore body

✉ *Corresponding author: Abdel-raheemkhalifa.12@azhar.edu.eg (A. Embaby)*

of Choghart in the Yazd Province of Iran. The deposit was classified into four homogenous zones, and the analysis was performed on each zone as well as the whole zone. The results show that the ANNs performed on the four zones were effectively higher than the ANNs applied to the overall ore body. [8] employed support vector machine (SVM) and ANN methods to characterize the organic richness of the source rock from well log data. The results from ANN and SVM decreased the computational time, and highly repeatable results were obtained.

Radioactive concentrations in Hazar Lake in Turkey were studied by [5] using an ANN model and geographical maps. The ^{226}Ra, ^{232}Th, and ^{238}U activity concentrations in water samples collected from the lake were 1.439 Bq/L, 4.508 Bq/L, and 14.682 Bq/L, respectively. The generated results have mean square errors that are fewer than 1.5%. The model for this investigation is valid, as evidenced by the correlation coefficient being near +1.

[9] used the ANN method to determine the link between the concentration of radon and various geo-physical, geological, and climatic characteristics that affect gas emissions from soil ^{222}Rn data collected over a period of seven years in Campi Flegrei, an Italian volcanic caldera near Naples. The results show that radon follows the times of caldera agitation, as shown by a comparison with earlier investigations using different methodologies, and that the ANN method is effective.

Various quantities of radioactive materials are contained in geological structures, and the source of this natural radioactivity is the existence of radionuclides in the earth's crust. Among these radioactive materials is uranium, of which nearly all uranium is present in nature as the isotope U^{238}. Uranium minerals are formed as a result of combining with different processes. It is found in almost all types of rocks and water in trace quantities [17], [18], [19] and[20]. Uranium ore in Gattar-V (G-V), located in the G. Gattar area, is associated with granite and Hammamat sediment rocks. Uranium ore deposits in the studied area have been examined by the Egyptian Nuclear Materials Authority (ENMA).

The goal of this work is to propose, firstly, a new empirical correlation based on non-linear multiple regression (NLMR), and secondly, a new ANN-based model to determine the U concentration as a function of thorium and total gamma-ray contents in Gattar-V (G-V) U occurrences.

2. Location and Geologic Setting

The studied area is located about 35 kilometers west of Hurghada city on the Red Sea coast, which is a part of the G. Gattar area, in the Egyptian Eastern Desert. (Figure 1). The studied area is bounded by latitudes 27° 07' 00" and 27° 07' 47" N and longitudes 33° 16' 50" and 33° 18' 00" E.

The G. Gattar area is located in the North Estern Desert of Egypt; it is deserted, and is mostly covered by basement rocks. As part of the G. Gattar area, the G-V uranium occurrence is mostly hosted in late Neoproterozoic granite with accompanying dikes and veins, as well as late Precambrian Hammamat sedimentary rocks (HSR) [21], [22] and [23]. Previous geological investigations classified these rock types as HSR (oldest), Gattar granite, acidic dikes, and basic dikes (youngest) in order of their age (Figure 2).
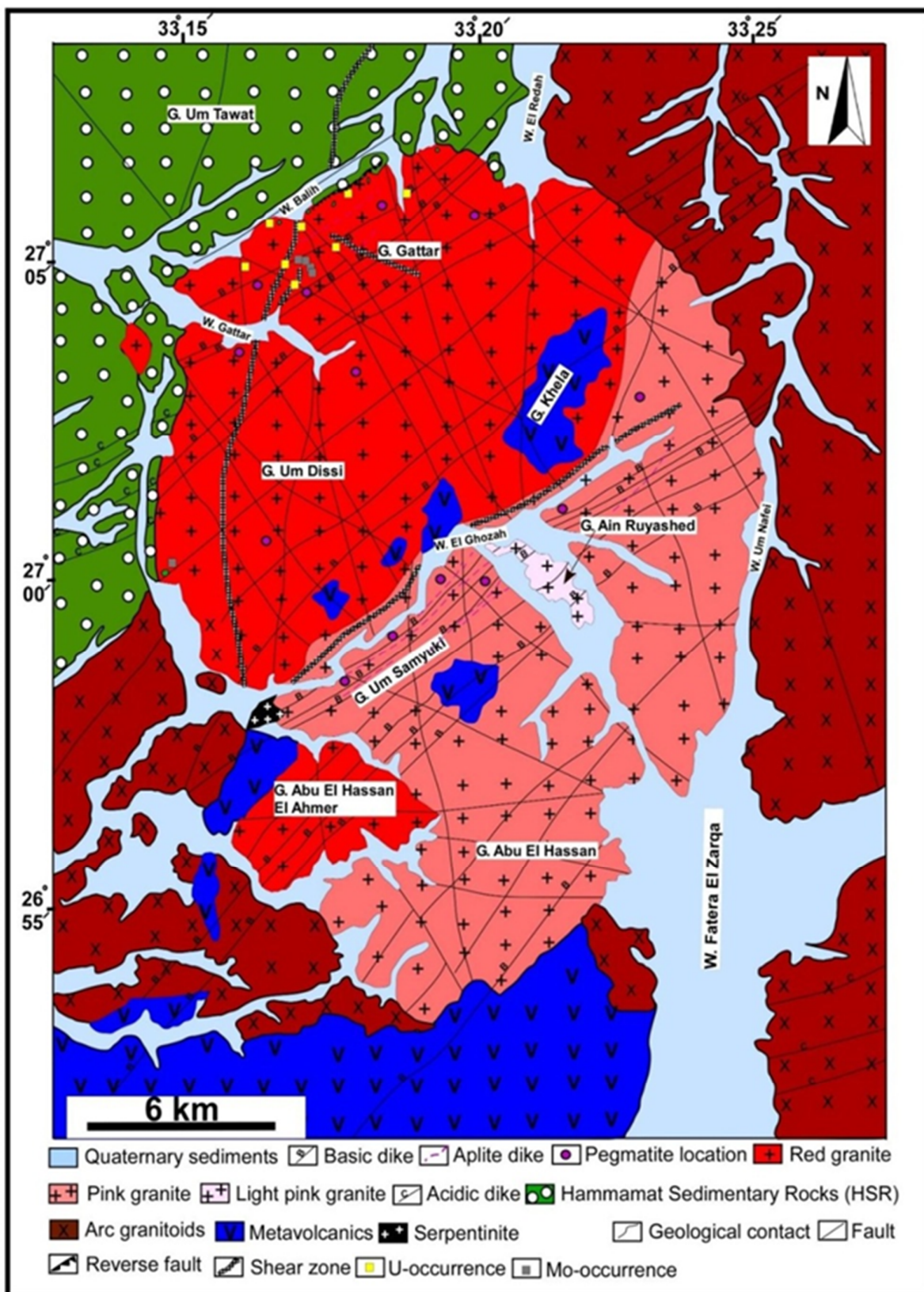
Figure 1. Geological map of Gattar granite, showing the country rocks location of the mineralized site aftar [24].
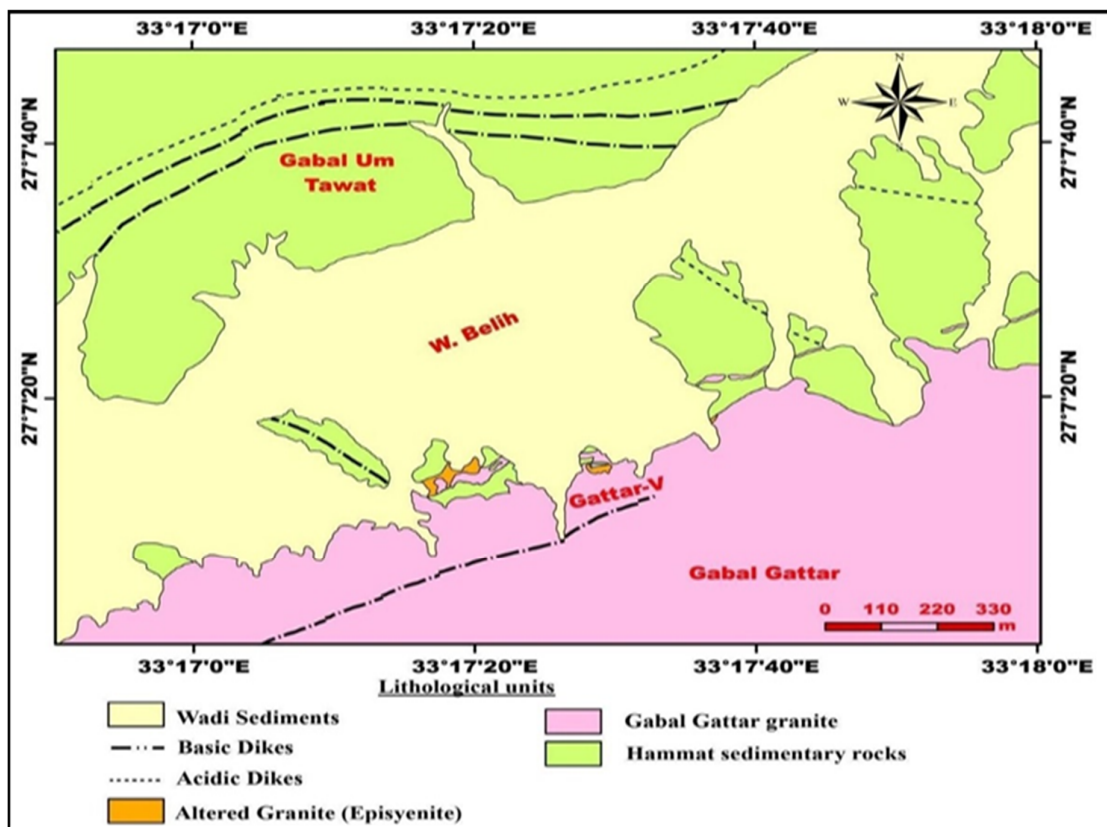
Figure 2. Deatiled geological map of G – V occurrence after [25] and [26].

G-V uranium occurrence can be considered a possible potential deposit for uranium, thorium, and yattrium (U, REE, and Y) and other rare metals mineralization. The mineralizations are caused by alkaline and oxidizing hot fluids, with the contribution of meteoric water. The hot fluids flowed up along the ENE-WSW and NE-SW faults to cause a rather complicated series of metasomatic reactions. The rare metals were mobilized from the younger granite pluton of Gattar and concentrated at the contact with Hammamat sediments. The reaction of the mineralizing solutions with the wall rocks and the pseudomorphic oxidation of pyrite caused the reduction and fixation of uranium [27]. [28] and [29] used the X-ray diffraction technique to identify uranophane and tyuyamunite as secondary uranium minerals in the studied area.

The mineralizations are structurally controlled and located along the contact shear zone of the W. Belih area, where they record a complex history of deformations. The uranium mineralization is located along the footwall of a shear zone striking ENE-WSW to NE-SW and dips $45°$- $73°$ to SE. This shear zone was reactivated during its tectonic history, starting from compression trending NW-SE and NE-SW, respectively, to younger extensional events trending NW-SE [30]. Detailed subsurface structural studies of GV occurrence in mining works revealed the presence of major sub-surface uranium mineralized trends recorded in the main fracture, and the fualts mostly had ENE-WSW and NE-SW directions in the mine [31].

3. Methodology of Study
3.1. Data gathering
3.1.1 Measurements and field data gathering

In the current research work, the fieldwork has been completed with the geologist of the G. Gattar project to complete the lacking geological information. Gamma-ray measurements, sampling for geo-chemical analysis and small-scale documentation for the radioactive anomaly zones are all included in this data.

At this occurrence, a grid with intervals of X axis = 20 meters and Y axis = 10 meters is carried out, covering a space that is 320 meters wide and 720 meters long (Figure 3). The profiles have a N27°W direction, running through the HSR in the north, crossing the contact zone between G. Gattar granite and Hammamat sediments. This grid is primarily used to monitor topography and radioactivity. The total number of these points is 1221, where uranium and thorium are expressed in equivalent concentrations (eU and eTh).
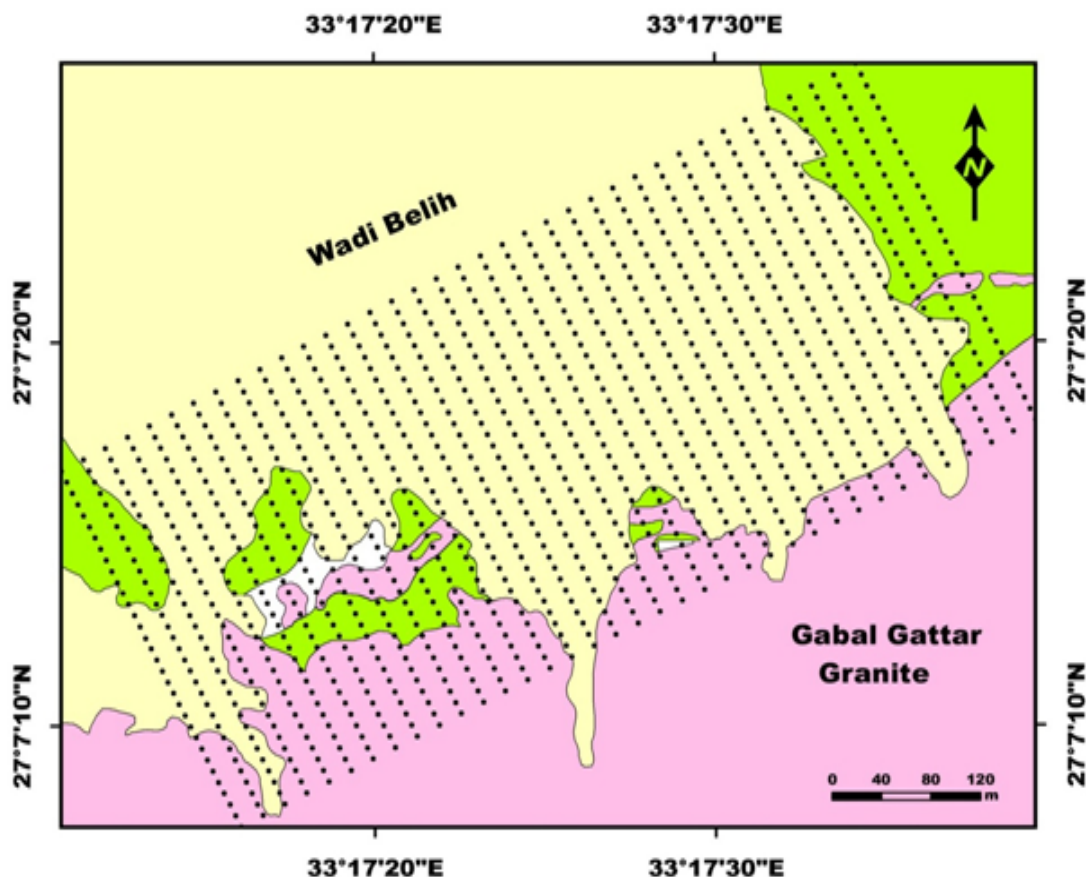
Figure 3. The grid pattern for 1221 datasets that are constructed in the G-V uranium occurrence, G. Gattar area.

3.1.2. Radioactivity

Data point coordinates, rock type, total gamma-ray (cps), eU (ppm), and eTh (ppm) are utilized in this work. Radioactivity is the result of the spontaneous disintegration of some unstable atomic nuclei. The nucleus produces alpha and beta particles, as well as electromagnetic rays, during this process. Natural background radioactivity is produced by the combined decay of uranium (U^{238}, U^{235}, and U^{234}), thorium (Th^{232}), and potassium (K^{40}) isotopes that emit gamma rays. Gamma-ray radiation measurement, which is the most practical approach for radiometric exploration surveys, is required for detection by different apparatuses. In the field, scintillometers are used to detect and measure gamma-ray intensity. Total gamma-ray radiation is detected in the field using a portable gamma-ray scintillometer detector, model RS-230 (Figure 4), which detects total gamma-ray in counts per second (cps), eU part per milion (ppm), and eTh (eTh) (ppm). The spectrometer was calibrated in the NMA's laboratory. An exhaustive ray survey is performed on the different rock types in the research region, inside the specified grid pattern, to detect surface concentrations of radio elements.

Figure 4. Field *in situ* measurements of gamma activity by a scintillometer detector (model RS-230).

3.1.3. Statistic evaluation

The G-V occurrence is a part of the G. Gattar area that is loacted in the northern part of the Egyptian Eastern Desert, where 1221 datasets were measured. The statistical analysis shown in Table 1 reveals the extensive range of the used data, with total γ-ray values ranging from 140 to 349 (ppm), eTh content values ranging from 5 to 38.9 (ppm), and **eU** values ranging from 4 to 37.9 (ppm). Figure 5 displays the 0.83 correlation coefficients between the output parameter (uranium content) and the input parameters (total gamma-ray and thorium content), respectively. The coefficient of correlation is used to measure how strong a relationship is between two variables. There are several types of coefficients of correlation, but the type used in this paper is Pearson's. Pearson's coefficient of correlation is commonly used in linear regression. To calculate Pearson's coefficient of correlation, we use this equation:

$$r = \frac{n\sum(xy) - (\sum x)(\sum y)}{\sqrt{[n\sum x^2 - (\sum x)^2][n\sum y^2 - (\sum y)^2]}} \quad (1)$$

Table 1. The datasets used in the investigation.

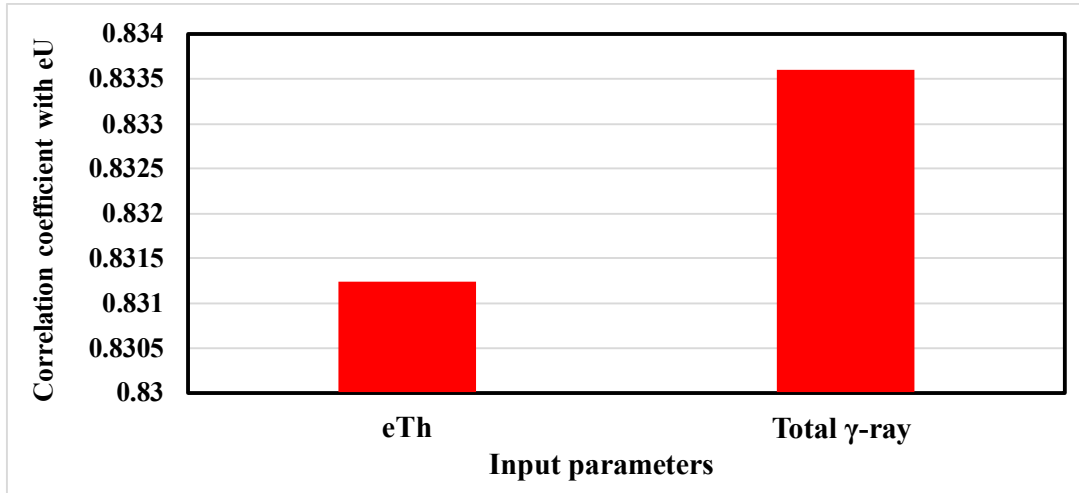| Statistical parameters	total γ-ray(cps)	eTh (ppm)	eU (ppm)
Mean	227.1	21.26	12.75
Standard error	1.45	0.23	0.15
Median	219	21.7	12.9
Mode	216	12.2	7.2
Standard deviation	50.78	8.12	5.31
Sample variance	2578.56	65.93	28.22
Kurtosis	-0.4	-0.84	3.07
Skewness	0.63	-0.03	1.06
Range	209	33.9	33.9
Minimum	140	5	4
Maximum	349	38.9	37.9
Count	1221	1221	1221

Figure 5. Correlation coefficients between eU (ppm) and input parameters (total γ-ray (cps) and eTh (ppm)).

3.2. Development of new correlation using NLMR

Using non-linear multiple regression (NLMR) to determine the uranium concentration as a function of thorium and total gamma, a novel mathematical association was given in this paper. Seventy percent (855 datasets) were used for training the model, and 366 datasets (30%) were used for validation and testing the model.

The developed correlation can be expressed as:

$$U_R = a_0 + a_1 G + a_2 T + a_3 G^2 + a_4 T^2 + a_5 G^3 + a_6 T^3 + a_7 GT + a_8 G^2 T + a_9 GT^2 \tag{2}$$

The coefficients of the suggested correlation are shown in Table 2. With a 0.99 determination coefficient, 3.85 standard deviation, 0.518 RMSE, -0.22% average percentage error, and 2.61% average absolute percentage1 error. This connection accurately predicts the uranium content. Figure 6 displays the cross-plots that analyze the behavior of this correlation. For hand calculations that facilitate and give a quick picture of the uranium content, this correlation can be used.

Table 2. NLMR-based proposed correlation coefficients.

a_0	72.85978	a_5	0.000011
a_1	-0.870365	a_6	-0.00392
a_2	4.650621	a_7	0.000059
a_3	0.000897	a_8	-0.00022
a_4	-0.057115	a_9	0.001628

3.3. Development of ANN-based empirical model

An ANN-based empirical model was proposed to calculate the U concentration as a function of total γ-ray and Th concentration. For this model, 855 datasets (70 percent of total datasets) were used for training, and 366 datasets (30 percent) were used for validation and testing. We examined the tan-sigmoid function of various numbers of hidden neurons in order to reach the best model. The pure-linear output function and the Levenberg-Marquardt training algorithm were both chosen in this approach.

3.4 Levenberg-Marquardt technique

An optimization method called the Levenberg-Marquardt Technique (LMT) was used to handle non-linear least squares issues. These miniaturization issues are particularly prevalent when fitting least-squares curves. The Gauss-Newton Algorithm (GNA) and the gradient color (GC) technique are interpolated by LMT. Since LMT is more resilient than GNA, it frequently finds a solution even when it begins very far from the final minimum. LMT typically runs slower than GNA for well-behaved functions and suitable beginning values. In many software programs, LMT is utilized to address general curve-fitting issues. It frequently converges more quickly with GNA than first-order techniques. LMA only discovers a local minimum, not necessarily a global minimum, like other iterative optimization techniques [32].
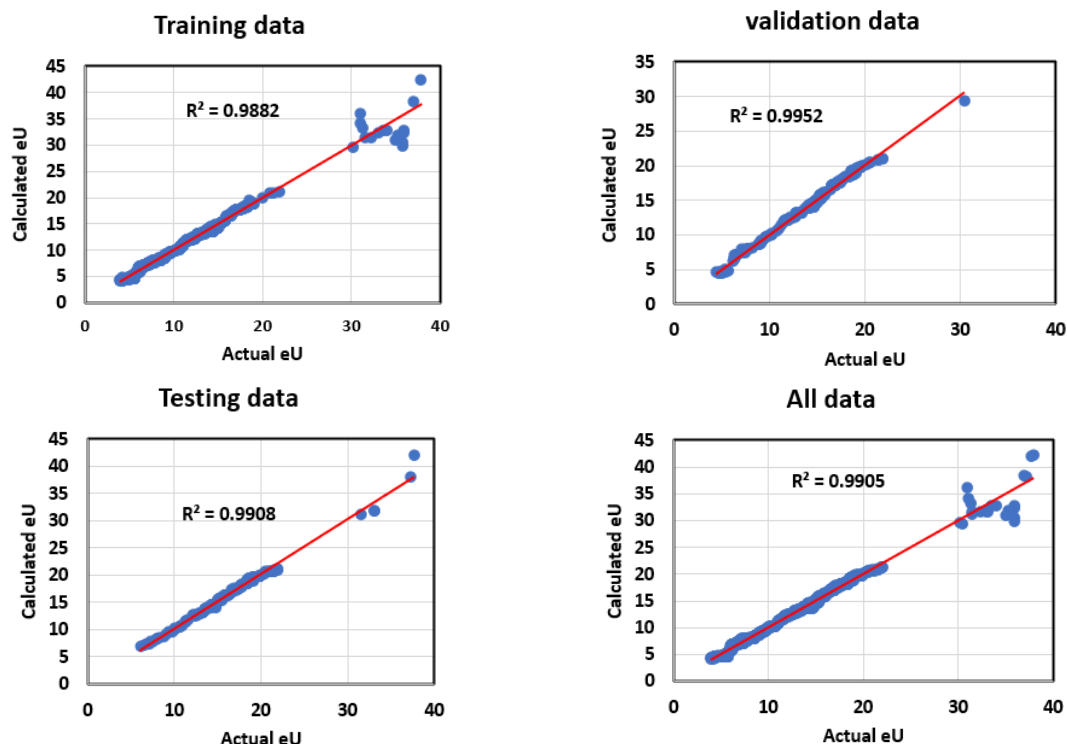
Figure 6. Using the suggested NLMR-based colouring, compare the estimated data with the actual data for eU (ppm).

4. Findings and Analysis
4.1. TIN forecasting maps of total gamma radioactivity, equivalent uranium, and equivalent thorium

The Geographic Information System (GIS) software projected the triangulated irregular network (TIN) map of total gamma radiation in G. Gattar based on 1221 datasets in Figure 7. It is possible to pinpoint exactly where the total gamma radiation is high and low in G. Gattar, as well as where it is distributed. As can be seen in Figure 7, the total gamma radioactivity of the G. Gattar ranged from 140 to 349 cps, showing localized total gamma radioactivity, particularly in the south and southwest.

While Figure 8 shows a TIN map of eU in G. Gattar that an ARc map, the GIS program predicted. It is possible to pinpoint exactly where high and low eU areas are located in G. Gattar, as well as where they are distributed. According to

Figure 8, the eU of the G. Gattar ranged from 4 to 37.9 ppm, showing selective eU in various places, particularly in the areas of the south and south-west, as well as the south-east, whereas the area of the east had a low concentration.

The TIN map of eTh in G. Gattar shown in Figure 9 was predicted using a GIS program. It is possible to pinpoint exactly where total gamma activity is high and low in G. Gattar, as well as where it is distributed. The equivalent thorium of the G. Gattar ranged from 5 to 38.9 ppm, as shown in Figure 9, showing selective eTh in various places, particularly in the areas of the south and south-west, as well as the south-east, whereas the area of the east had a low concentration.

This behavior demonstrates the concentration of eU and eTh in the total gamma radiation. As a result, this can assist project engineers in forecasting the high and low activity levels in G. Gattar as well as in determining whether or not the area will need to be developed for industry.
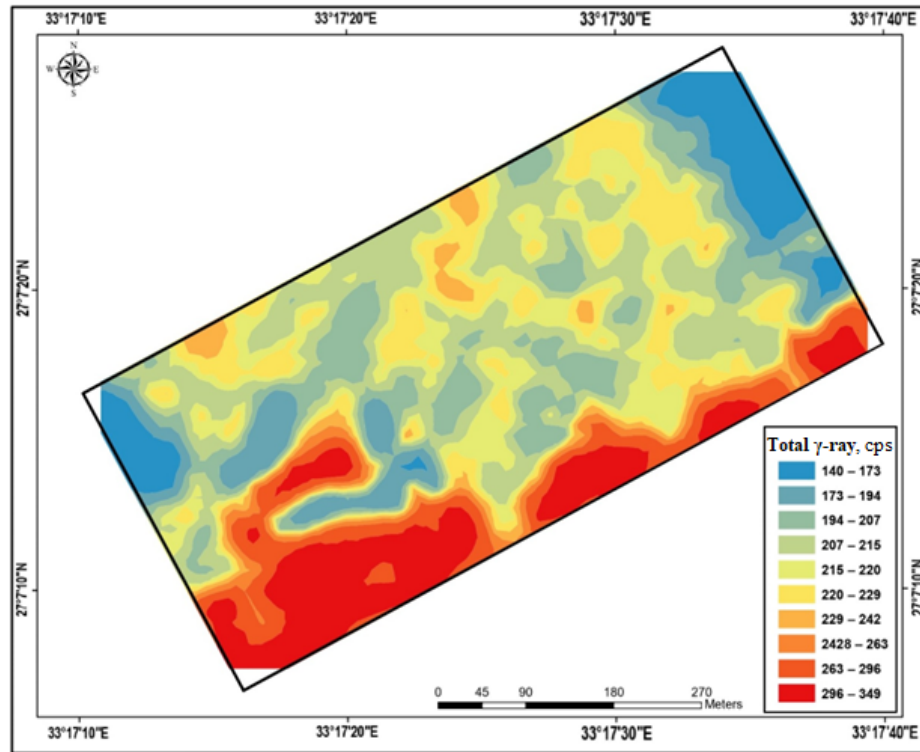
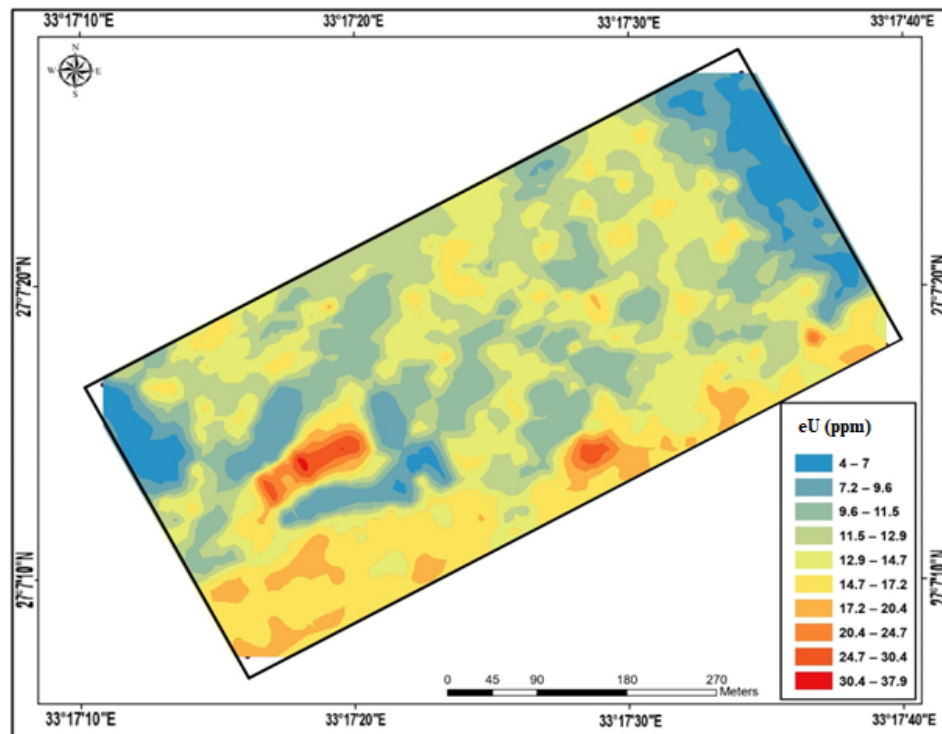**Figure 7. Map for prediction of the total gamma radioactivity concentrations (cps) measured over 1221 points.**

Figure 8. Map for prediction of the eU concentrations (ppm) measured over 1221 points.
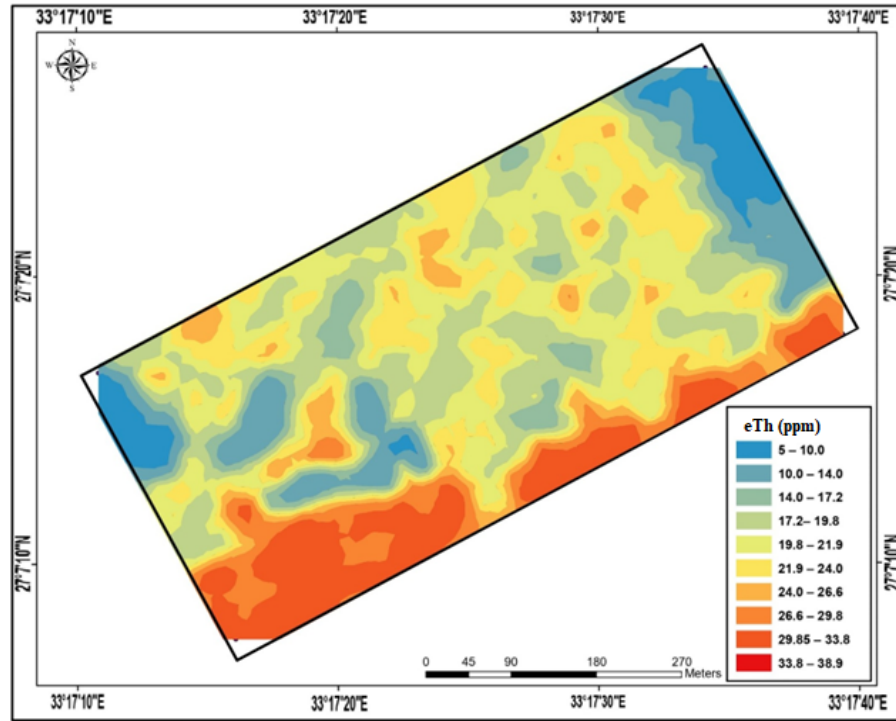
Figure 9. Map for prediction of the eTh concentrations (ppm) measured over 1221 points.

4.2. Model enhancement and description

The input layer, hidden layer, and output layer are all parts of the suggested model. The total γ-ray and Th content are the two neurons that make up the input layer's input parameters. There are eight neurons in the buried layer. One neuron for the output parameter, the U content, is present in the output layer. We investigated the tan sigmoid as a transfer function for various numbers of hidden neurons (4, 5, 6, 7, 8, 9, and 10) in order to arrive at the ideal ANN model, as shown in Table 3. We discovered that n = 8 had both the highest coefficient of determination and the lowest RMSE. To prove this, a Levenberg-Marquardt technique was chosen as the training procedure, and the output function's pure-linear function was scrutinized. The characteristics of the suggested models are listed in Table 4, and Figure 10 (a, b) depicts the recommended ANN model's architectural layout.

Table 3. Evaluation of model accuracy at various numbers of hidden-layer neurons.

	Four neurons	Five neurons	Six neurons	Seven neurons	Eight neurons	Nine neurons	Ten neurons
R^2	0.997139	0.999028	0.997422	0.99784	0.999529	0.998401	0.999343
SD	3.429524	1.705442	3.102467	2.239395	1.203021	1.906754	1.539997
RMSE	0.283365	0.165337	0.267381	0.246299	0.115109	0.212715	0.13593
RE	-0.3403	-0.00401	-0.13114	-0.00786	-0.07779	-0.05588	-0.09827
AE	1.963738	1.154657	1.969398	1.387439	0.761271	1.145853	0.959828

Table 4. Features of the suggested ANN model.

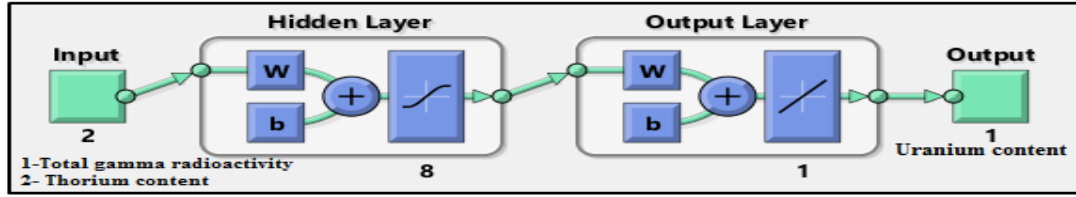| Parameter	Value
Model layers	Three
Neurons of the input layer	Two
Neuronsof hidden layer	Eight
Optimization technique	Levenberg-Marquardt
Activation function of hidden layer	Tan-Sigmoid
Transfer functionof output layer	Pure-linear

Figure10 a. The suggested architecture of the ANN model for computing uranium content.
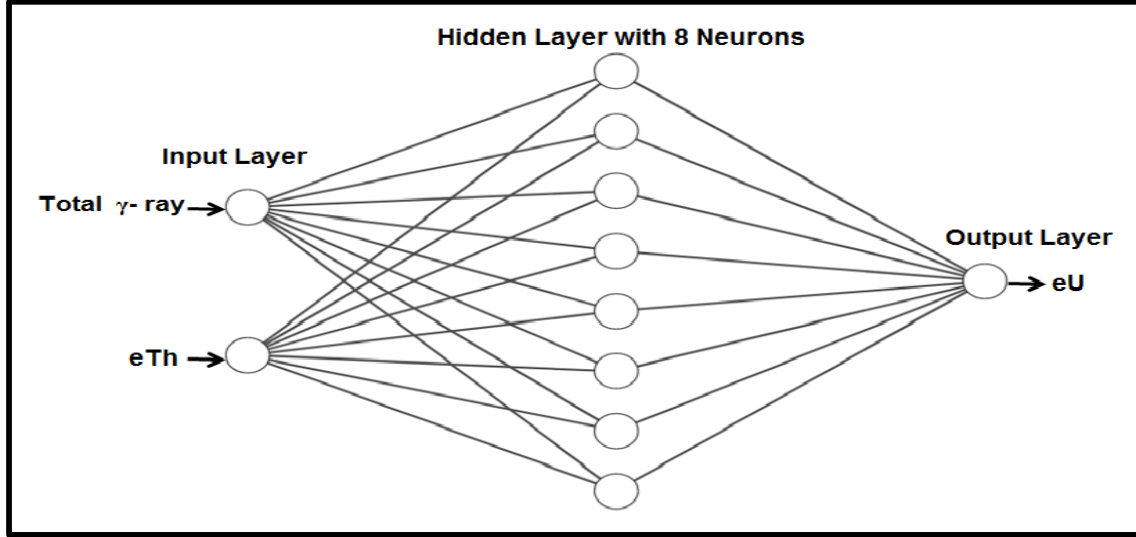

Figure10 b. The suggested architecture of the ANN model for computing uranium content.

4.3. Suggested ANN model

We substitute real GR and Th content in the following equations (Eqs. 3 and 4) to normalize them to be used in Equeation 5.

$$GR_n = 0,009569 GR - 2,339713 \qquad (3)$$

$$TH_n = 0,058997 eTh - 1,294985 \qquad (4)$$

The inputs of the selected eighth hidden layer are calculated using the following formula using the normalized parameters for each dataset and the neuron-specific model coefficients (Table 5):

$$S_i = GR_n W_{i1} + TH_n W_{i2} + b \qquad (5)$$

To determine the U content for each dataset, the following mathematical expression can be used:

$$U_R = 16,95 \left[\sum \left(\frac{2}{1 + e^{-2 \times S_i}} - 1 \right) w_{hi} + b_h \right] + 20,95 \qquad (6)$$

Table 5. The proposed model's coefficients.

i	w_1	w_2	b	w_h	b_h
1	-1.542	2.4188	5.096	0.8786	1.2144
2	-0.7686	-0.313	1.2914	-1.117	
3	6.4385	-7.324	-2.379	1.8542	
4	4.8988	-6.764	-1.736	-1.316	
5	10.005	-5.89	1.9553	0.4661	
6	-7.0944	2.1264	-4.524	-1.815	
7	3.6362	-2.573	0.9424	-0.998	
8	-1.7142	-2.094	-3.419	2.5518	

Figure 11 depicts the calculated values of uranium content as a function of the actually measured ones. All the data points fall near the unit-slope straight line with coefficients of determination values greater than 0.999. This indicates that the proposed model is a reliable predictive tool.

The use of the neural network method is justified from two reasons: first, this study proves the ability to develop an ANN-based empirical correlation capable of predicting the uranium content. Second, the ANN-based correlation is more accurate to predict the uranium content, especially in large datasets.
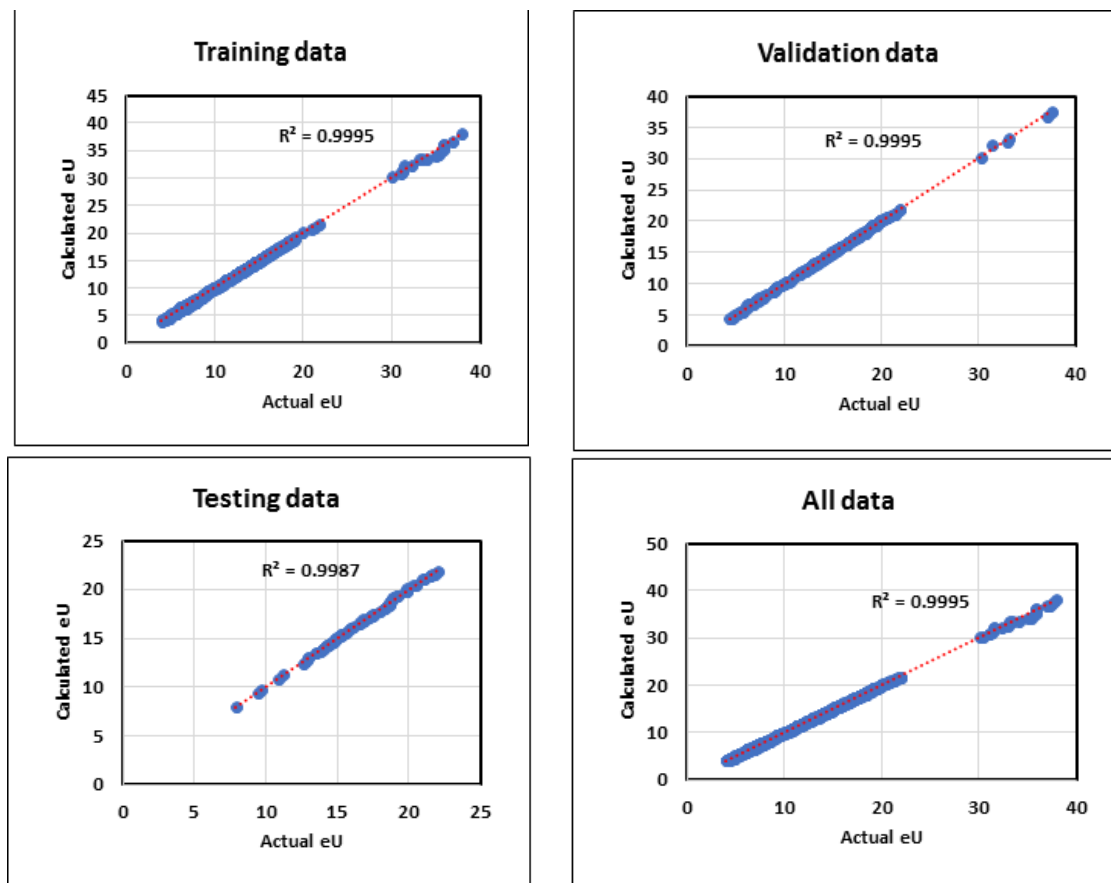

Figure 11. Cross-plots of training, validation, and testing of the proposed model for eU (ppm).

5. Conclusions

From this work, the following conclusions can be drawn:

During orecast concentration maps, using GIS in the G-V located in the G. Gattar area of the Eastern Desert of Egypt, total gamma, eU and eTh map analyses were successfully built, allowing the low and high concentrations to be identified. The high concentration of total gamma radioactivity in the studied area is located in the south and south-west. Uranium is concentrated in different parts of the studied area. In the south parts, they show a high concentration, while it shows a low concentration in the east of the studied area. Thorium shows a high concentration in the south, south-west, and south-east parts of the studied area, but it shows a low concentration in the east of the

studied area. For the purpose of forecasting uranium concentration as a function of the total γ-ray and thorium contents, a non-linear multiple regression (NLMR)-based model was created. The results show that the determination coefficient (R^2) between the estimated and actual eU was 0.99. This correlation was used to simplify and provide a fast overview of uranium through manual computations. In addition, a complete ANN-based approach was presented to determine the uranium concentration as a function of thorium and total γ-ray contents, where ANNs are very accurate. The proposed model is a fast, reliable, not expensive, and powerful predictive tool. This model can be used through software for more accurate results. Moreover, any alternative dataset from a different place may be used with the proposed models.

Acknowledgment

References

[1]. Dragovic, S., Onjia, A., Stankovic, S., Anicin, I., and Bacic, G. (2005). Artificial neural network modelling of uncertainty in gamma-ray spectrometry. *Nuclear Instruments and Methods in Physics Research, 540 (2-3)*, 455-463.

[2]. Al-Bulushi, N. I., Peter Robert King., Blunt, M. J., and Kraaijveld, M. (2012). Artificial neural networks workflow and its application in the petroleum industry. *Neural Computing and Applications, 21*, 409-421. doi 10.1007/s00521-010-0501-6

[3]. IAEA. (2007). Naturally occurring radioactive material. *Proceedings of an International Symposium Held in Seville, Spain*, pp.297-306.

[4]. UNSCEAR. (1988). Sources, effects and risks of ionizing radiation united nations scientific committee on the effects of atomic radiation 1988 report to the general assembly with annexes. *United nations, New York*, 647 P.

[5]. Sevim B., Mirac K., Ahmet B., and Fatih K. (2018). Forecasting of Ra-226, Th-232, and U-238 concentrations using artificial neural networks (anns). *Cumhuriyet Science Journal,39-1*, 87-94.

[6]. Rigo-J.P., Chica O. M., and Abarca F. (2003). Artificial neural networks as a tool for mineral potential mapping with GIS. *International Journal of Remote Sensing, 24*, 1151–1156.

[7]. Nezamolhosseini, S.A., Mojtahedzadeh, S.H., and Gholamnejad, J. (2017). The application of artificial neural networks to ore reserve estimation at Choghart Iron ore deposit. *Analytical and Numerical Methods in Mining Engineering, 6*, 73-83.

[8]. Bolandi, V., Kadkhodaie, A., and Farzi, R. (2017). Analyzing organic richness of source rocks from well log data by using SVM and ANN classifiers: A case study from the Kazhdumi formation, the Persian Gulf basin, offshore Iran. *Journal of Petroleum Science and Engineering, 151*, 224-234.

[9]. Ambrosino, F., Sabbarese, C., Roca, V., Giudicepietro, F., and Chiodini, G. (2020). Analysis of 7-years radon time series at Campi Flegrei area (Naples, Italy) using artificial neural network method. *Applied Radiation Isotopes, 163*, 109239. https://doi.org/10.1016/j.apradiso.2020.109239 [10]. Yasrebi, A.B., Hezarkhani, A., Afzal, P., Karami, R., Eskandarnejad Tehrani, M., and Borumandnia, A. (2020). Application of an ordinary kriging-artificial

neural network for elemental distribution in kahang porphyry deposit, central Iran. *Arabian Journal of Geosciences, 13(748)*, 1-14.

[11]. Afzal, P., Farhadi, S., ShamseddinMeigooni, M., BoveiriKonari, M., and Daneshvar Saein, L. (2022). Geochemical anomaly detection in the irankuh district using hybrid machine learning technique and fractal modeling. *Geopersia, 12(1)*, 191-199. doi: 10.22059/GEOPE.2022.336072.648644

[12]. Farhadi, S., Afzal, P., BoveiriKonari, M., Daneshvar Saein, L., and Sadeghi, B. (2022). Combination of machine learning algorithms with concentration-area fractal method for soil geochemical anomaly detection in sediment-hosted irankuh pb-zn deposit, central Iran. *Minerals, 12 (6)*, 689. https://doi.org/10.3390/min12060689

[13]. Amit Kumar Gorai1, Simit Raval, Ashok Kumar Patel, Snehamoy Chatterjee, and Tarini Gautam. (2021). Design and development of a machine vision system using artificial neural network-based algorithm for automated coal characterization. *International Journal of Coal Science &Technology, 8(4)*,737–755.

[14]. Sevim Bilici, Mirac Kamislioglu, Ahmet Bilici, and Fatih Kulahci. (2018). Forecasting of Ra-226, Th-232, and U-238 concentrations using artificial neural networks (ANNs). *Cumhuriyet Science Journal, 39-1*, 87-94.

[15]. Snezana Dragovic. (2022). Artificial neural network modeling in environmental radioactivity studies – A review. *Science of the Total Environment, 847*, 157526.

[16]. Cody A. Nizinski, Cuong Ly, Clement Vachet, Alex Hagen, TolgaTasdizen, and Luther W. McDonald IV. (2022). Characterization of uncertainties and model generalizability for convolutional neural network predictions of uranium ore concentrate morphology. *Chemometrics and Intelligent Laboratory Systems, 225*, 104556.

[17]. Külahci F. Spatiotemporal. (2016). four-dimensional modeling and simulation of uranium (238) in Hazar Lake (Turkey) water. *Environmental Earth Sciences, 75(452)*.

[18]. Ambrosino, F., Stellato, L., and Sabbarese, C. (2020). A case study on possible radiological contamination in the Lo Uttaro landfill site (Caserta, Italy). *Journal Physics Conferance Series, 1548*, 012001. doi: https://dx.doi.org/10.1088/1742-6596/1548/1/012001

[19]. Fabrizio Ambrosino, Lenka Thinová, Miroslav Hýža, and Carlo Sabbarese. (2020). ^{214}Bi/^{214}Pb radioactivity ratio three-year monitoring in rainwater in Prague. *Nukleonika, 65(2)*,115–119. doi: 10.2478/nuka-2020-0018

[20]. Shalaby, M. H. (1990). Uranium mineralization in the northern Gabal Qattar locality, Northern Eastern

Desert. *7th Conferance Phanerozoic and Development, Al Azhar University, Cairo, Egypt,* 3-19.

[21]. Závodská L., Kosorínová E., Ščerbáková L., and Lesný J (2008). Environmental Chemistry of Uranium. *Hej, Env-081221-A,* 1-19. http://heja.szif.hu/ENV/ENV-081221-A/env081221a.pdf

[22]. Roz., M. E. (1994). Geology and uranium mineralization of Gabal Gattar area, North Eastern Desert, Egypt. *M.Sc. Thesis, Faculty of Science, Al Azhar University, Cairo, Egypt.*

[23]. Abu Zaid., M. M. (1995). Relation between surface and subsurface uranium mineralization and structural features, Gebel Gattar, North Eastern Desert, Egypt. *M.Sc. Thesis, Ain Shams University, Cairo, Egypt.*

[24]. Mahdy., N. M. (2015). A genetic model for molybdenum and uranium mineralization in Gebel Gattar Granite, North Eastern Desert, Egypt. *M.Sc. Thesis, Ain Shams University, Cairo, Egypt.*

[25]. Waheeb, A. G. (2021). Resolved shear for the uranium mineralized fault contacts at Gabal Abu Hamr and Gabal Gattar, northern eastern desert, Egypt. *Annals of Geological Survey of Egypt. V. XXX VIII,* 243-255.

[26]. Yehia Z. Darwish, A. Kh Embaby, Mohamed A. El Zalaky, Darwish M. El Kholy, and Samir M. Selim. (2022). Arbitrary estimation of uranium ore reserves in Qattar–V, Northeastern Desert, Egypt using geographic information system. *Journal of Radiation Research and Applied Sciences, 15,* 224–231. https://doi.org/10.1016/j.jrras.2022.01.022

[27]. El-Kammar, A.M., Salman, A.E., Shalaby, M.H., and Mahdy, A.I. (2001). Geochemical and genetical constraints on rare metals mineralizations at the central Eastern Desert of Egypt. *Chemical Journal, 35,* 117–135. https://www.jstage.jst.go.jp/article/geochemj1966/35/2/35_2_117/_pdf

[28]. Mahdy, M.A., Salman, A.B., and Mahmoud, A.H. (1990). Leaching studies on the uraniferous Hammamat sediments, Wadi Bali, northern estern desert, Egypt. *14th Congress of Mining and Metallergy, Edinburgh Scotlafd,* 229-235.

[29]. Mahdy, A.A. (1999). petrological and geochemical studies on the younger granites and hammamat sediments at Gabal Gattar-5 uranium occurrence, wadi Balih, North Easter Desert, Egypt. *PhD Thesis, Geology Department, Faculty of Science, Ain shams University, Cairo, Egypt.*

[30]. Waheeb, A.G. and El Sundoly, H.I. (2016). Structure roles for the localization of metasomatite uranium deposit type at wadi Belih area, Northern Eastern Desert, Egypt. *Egyptian Journal of Petroleum, 25,* 201-214.

[31]. Amin, N.F. (2010). Surface and sub-surface structural features controlling uranium mineralizations at granitic-hammamat contact, Wadi Belieh, Northern Eastern Desert, Egypt. *PhD Thesis, Faculty of Science, Ain Shams University, Cairo, Egypt.*

[32]. Binu, D. and Rajakumar, B. R. Eds.(2021). Artificial intelligence in data mining: Theories and applications. *Elsevier Science and Technology, Academic Press, India,* 257 P. https://www.researchandmarkets.com/reports/5203956/artificial-intelligence-in-data-mining-theories.

پیش‌بینی محتوای اورانیوم گابل‌گتار به عنوان تابعی از محتویات کل اشعه گاما و توریم با استفاده از یک شبکه عصبی مصنوعی در صحرای شمال شرقی، مصر

عبدالرحیم امبابی[۱]*، سید گماء[۱]، یحیی درویش[۱,۲]، و سمیر سلیم[۱]

۱. گروه مهندسی معدن و نفت، دانشکده فنی، دانشگاه الازهر، قاهره، مصر

۲. سازمان مواد هسته‌ای، P.O. 530 المادی، قاهره، مصر

* نویسنده مسئول مکاتبات: pporchelvan@vit.ac.in

چکیده:

این مطالعه با هدف توسـعه یک مدل همبسـتگی تجربی برای تخمین محتوای اورانیوم G-V در منطقه گابل گتار، صحرای شـمال شـرقی مصـر، به عنوان تابعی از محتوای توریم و کل اشعه گاما است. با استفاده از نرم افزار متلب، تأثیر انتخاب tan-sigmoid به عنوان تابع انتقال در تعداد مختلف نورون‌های پنهان برای رسیدن به مدل بهینه شـبکه عصـبی مصـنوعی (ANN) مورد بررسـی قرار گرفت. تابع خطی خالص به عنوان تابع خروجی مورد بررسـی قرار گرفت و رویکرد لونبرگ-مارکوارت به عنوان تکنیک بهینه‌سازی انتخاب شـد. بر اسـاس ۱۲۲۱ مجموعه داده، یک همبسـتگی تجربی مبتنی بر ANN جدید برای محاسـبه مقادیر اورانیوم (U) ایجاد شـد. نتایج طیف وسـیعی از محتوای اورانیوم را با ضـریب تعیین (R2) حدود ۰.۹۹۹، ریشـه میانگین مربعات خطا (RMSE) برابر با ۰.۱۱۵٪، میانگین خطای نسبی ٪0.05- (MRE) و میانگین مطلق را نشان می‌دهد. خطای نسبی ٪0.76 (MARE). مقایسه نتایج به‌دست‌آمده با بررسی میدانی نشان می‌دهد که مدل ANN پیشنهادی عملکرد خوبی داشته است.

کلمات کلیدی: ANN، غلظت اورانیوم و توریم، پرتو گامای کل، مدل‌سازی، ناحیه گتار.